1-2024

Effect of Anisotropic Brain Conductivity on Patient-specific Volume of Tissue Activation in Deep Brain Stimulation for Parkinson Disease

Xiaoxuan Liu

Kevin L. Chou

Parag G. Patil

Karlo A. Malaga
Bucknell University, kam068@bucknell.edu

Effect of anisotropic brain conductivity on patient-specific volume of tissue activation in deep brain stimulation for Parkinson disease

Xiaoxuan Liu, Kelvin L. Chou, Parag G. Patil, and Karlo A. Malaga*

Abstract*—*Objective: **Deep brain stimulation (DBS) modeling can improve surgical targeting by quantifying the spatial extent of stimulation relative to subcortical structures of interest. A certain degree of model complexity is required to obtain accurate predictions, particularly complexity regarding electrical properties of the tissue around DBS electrodes. In this study, the effect of anisotropy on the volume of tissue activation (VTA) was evaluated in an individualized manner.** ***Methods:*** **Tissue activation models incorporating patient-specific tissue conductivity were built for 40 Parkinson disease patients who had received bilateral subthalamic nucleus (STN) DBS. To assess the impact of local changes in tissue anisotropy, one VTA was computed at each electrode contact using identical stimulation parameters. For comparison, VTAs were also computed assuming isotropic tissue conductivity. Stimulation location was considered by classifying the anisotropic VTAs relative to the STN. VTAs were characterized based on volume, spread in three directions, sphericity, and Dice coefficient.** ***Results:*** **Incorporating anisotropy generated significantly larger and less spherical VTAs overall. However, its effect on VTA size and shape was variable and more nuanced at the individual patient and implantation levels. Dorsal VTAs had significantly higher sphericity than ventral VTAs, suggesting more isotropic behavior. Contrastingly, lateral and posterior VTAs had significantly larger and smaller lateral-medial spreads, respectively. Volume and spread correlated negatively with sphericity.** ***Conclusion:*** **The influence of anisotropy on VTA predictions is important to consider, and varies across patients and stimulation location.** ***Significance:*** **This study highlights the importance of considering individualized factors in DBS modeling to accurately characterize the VTA.**

***Index Terms*—Anisotropy, deep brain stimulation, diffusion tensor imaging, electric field modeling, Parkinson disease, subthalamic nucleus, volume of tissue activation.**

Manuscript received November 19, 2022. This work was supported by the Swanson Fellowship in the Sciences and Engineering (K. A. M.) and the Program for Undergraduate Research (Dean's Fund for Summer Undergraduate Research in STEM) (X. L.) at Bucknell University.

X. Liu is with the Department of Biomedical Engineering, Bucknell University, Lewisburg, PA, USA. K. L. Chou is with the Departments of Neurology and Neurosurgery, University of Michigan, Ann Arbor, MI, USA. P. G. Patil is with the Departments of Neurology, Neurosurgery, and Biomedical Engineering, University of Michigan, Ann Arbor, MI, USA. *K. A. Malaga is with the Department of Biomedical Engineering, Bucknell University, Lewisburg, PA, USA (correspondence e-mail: karlo.a.malaga@bucknell.edu).

I. Introduction

DEEP brain stimulation (DBS) has shown tremendous promise in treating symptoms of movement disorders, such as Parkinson disease (PD) and essential tremor, and psychiatric disorders, such as obsessive-compulsive disorder and major depression [1], [2]. However, a better understanding of how DBS modulates pathological neural activity is needed to optimize the therapy for patients. Clinical outcomes are highly dependent on electrode location and stimulation parameter settings. An accurate representation of the spatial extent of stimulation relative to surrounding structures may help clinicians localize stimulation to the target region via electrode placement and parameter adjustment. The electric field induced by DBS can be modeled using finite element analysis (FEA) and then thresholded appropriately to estimate the amount of neural tissue directly modulated, termed the volume of tissue activation (VTA) [3], [4]. DBS modeling and the VTA are valuable tools for both mechanistic study and clinical application [5], [6]. For example, they can be used to quantify and visualize stimulation delivered to specific parts of the brain, interpret and predict outcomes, investigate different targets, and validate new DBS paradigms and electrode designs [7], [8].

Current techniques for modeling the VTA vary in their complexity and implementation. Simplifications are usually made due to constraints on computational time and capability [9], [10]. Although a certain level of complexity is required to obtain accurate predictions from DBS models, exactly how much complexity is necessary and what aspects should be prioritized are still unclear. Many relevant factors contribute to the complexity of the model (to different degrees) and influence its solution when solved (often the distribution of the electric potential and field) [11]. These factors include neuroanatomy [12], [13], electrode geometry [14], [15], lead trajectory [16], [17], electrical material properties [18], [19], electrode-tissue interface [20], and stimulation settings [21]. Regarding the tissue surrounding the lead, a common simplification is to assume that it is a homogeneous and isotropic medium despite its nonuniform material composition and properties. Previous studies have investigated the effect of incorporating more complex electrical tissue properties, such as heterogeneity and anisotropy, on VTA predictions [11], [18]–[20], [22]–[24]. Tissue anisotropy, in particular, was

identified as a key factor to consider in DBS modeling due to its sizable influence on the stimulation-induced field distribution [18]. However, the impact of anisotropy on the VTA has not been evaluated across a large cohort of patients.

The objective of the present study was to evaluate the effect of anisotropy on the VTA in an individualized manner based on patient-specific electrical tissue conductivity and stimulation location. Tissue activation models of STN DBS were used to assess the strength of this effect across PD patients. To the authors' knowledge, this study is the first to quantitatively analyze the influence of intra- and intersubject variability in tissue anisotropy on VTA size and shape at this large a scale (40 patients).

II. Methods

A. Patient Dataset

Patients were selected from a clinical database at the University of Michigan (U-M) [7]. Forty patients (28 male, 12 female) with advanced PD who had received bilateral STN DBS were included, yielding 80 lead implantations (model 3389, Medtronic plc, Minneapolis, MN, USA). Of the 80 implantations, eight leads that delivered nonmonopolar stimulation were excluded. Therefore, a total of 72 implantations (37 left hemisphere, 35 right hemisphere) were modeled, simulated, and analyzed in this study. Information about the patient dataset is summarized in Table I. Clinical data obtained for each patient consisted of preoperative magnetic resonance imaging (MRI), preoperative diffusion tensor imaging (DTI), postoperative computed tomography (CT), and therapeutic stimulation settings. Details regarding image acquisition and processing are described in [7]. Briefly, the MRI and CT were acquired using previously published imaging protocols [25]. Settings for the MRI included: field strength = 3 T, slice orientation = coronal, voxel size = 0.69 × 1.25 × 0.69 mm, slice thickness = 1.25 mm, and number of slices = 40. CT settings included: slice orientation = axial, voxel size = 0.5 × 0.5 × 0.625 mm, and slice thickness = 0.625 mm. DTI settings included: field strength = 3 T, number of orientations = 15, b-value = 800 mm^2/s, and voxel size = 1 × 1 × 2 mm. The MRI and DTI data were resampled using linear and cubic spline interpolation, respectively. At the end of image processing, all imaging data had a uniform voxel size of 0.51 × 0.51 × 0.51 mm. Use of the data for this study was approved in advance by the Institutional Review Boards at Bucknell University and U-M.

TABLE I
PATIENT DATASET INFORMATION

	Mean	SD	Range
Age (baseline) [yr]	63.1	6.7	52.7-74.7
Age (diagnosis) [yr]	52.9	8.6	33.0-69.0
Disease duration [yr]	10.3	5.2	2.0-22.8
DBS amplitude [V]	2.7	0.6	1.5-4.2
DBS frequency [Hz]	141.3	22.6	125-185
DBS pulse width [μs]	60.4	3.5	60-90

Number (patient) = 40 (28 M, 12 F), number (implantation) = 72 (37 L, 35 R); SD: standard deviation.

B. Individualized Tissue Activation Modeling

A 3D finite element model incorporating patient-specific neuroanatomy, lead position and orientation, anisotropic (and heterogeneous) tissue conductivity, and therapeutic stimulation settings was created for each implantation using COMSOL Multiphysics (5.5, COMSOL, Inc., Burlington, MA, USA) to simulate the electric field induced by DBS. Tissue activation models were built following the individualized (N-of-1) modeling framework described in detail in [7] (Fig. 1a). Briefly, STNs traced from coronal MRI slices and electrode coordinates measured from 3D CT reconstructions using Analyze (12.0, AnalyzeDirect, Inc., Overland Park, KS, USA) were imported into MATLAB (R2021, The MathWorks, Inc., Natick, MA, USA) for analysis. The anisotropic electrical conductivity of the tissue was estimated using the DTI data. More specifically, Analyze's Diffusion Tensor Imaging add-on was used to calculate diffusion eigenvalue and eigenvector maps. These maps were imported into MATLAB, where they were then transformed into diffusion tensors via matrix diagonalization [26]. The diffusion tensor fields were subsequently converted to conductivity tensor fields via a linear transformation [27]. Lastly, the conductivity tensors were imported into COMSOL for FEA (Supplement S.I).

The electric potential throughout the tissue was solved using the steady state continuity equation for electric current density:

$$\nabla \cdot \boldsymbol{J} = -\nabla \cdot (\sigma \nabla V) = 0, \tag{1}$$

where $\boldsymbol{J}$ is the current density, σ is the conductivity, and V is the electric potential. The electric field norm was calculated from the potential and thresholded to define the VTA. VTA thresholds were derived from biophysical neuron models oriented perpendicular to the lead, assuming an axon diameter of 2.5 μm and stimulation pulse width of 60 μs [4]. Thresholds varied based on the stimulation amplitude of the implantation modeled.

For each implantation, four simulations were run (one for each electrode) to assess the effect of local changes in anisotropy on the VTA (Fig. 1b, top). Between simulations, only the active electrode contact changed. All other model parameters stayed the same. This yielded a total of 288 anisotropic VTAs across 40 patients and 72 implantations. To serve as a baseline comparison, tissue activation models with a homogeneous and isotropic conductivity of 0.33 S/m for the entire bulk tissue domain [28] were also built for each implantation (Fig. 1b, bottom). Simulations for each electrode were not run because changing the active contact did not generate significantly different VTAs despite the lead geometry given the uniform tissue conductivity. Instead, the same isotropic VTA (corresponding to the therapeutic active contact) was associated with each electrode for each implantation. This yielded a total of 288 isotropic VTAs (of which 72 were unique).

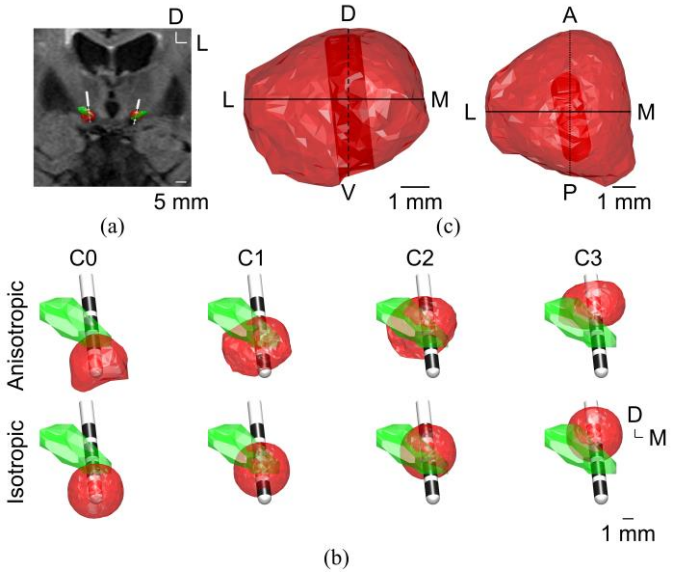

Fig. 1. Individualized tissue activation modeling and VTA characterization. (a) Coronal MRI slice for one patient showing the DBS lead and electrodes, STN (green), and VTA (red) in the left and right hemispheres. (b) Coronal view of the anisotropic (top) and isotropic (bottom) VTAs at each electrode contact (C0-C3) for one implantation. (c) Coronal (left) and axial (right) view of one anisotropic VTA showing spread measured in the lateral-medial (solid line), anterior-posterior (dotted line), and dorsal-ventral (dashed line) directions. L, M, A, P, D, and V correspond to the lateral, medial, anterior, posterior, dorsal, and ventral directions, respectively.

C. VTA Size and Shape Characterization

Anisotropic and isotropic VTAs were characterized based on size using the following metrics: volume and lateral-medial (LM), anterior-posterior (AP), and dorsal-ventral (DV) spreads. LM and DV spreads were measured in the coronal plane at the center of the VTA (Fig. 1c, left). Similarly, AP spread was measured in the axial plane (Fig. 1c, right).

VTAs were also characterized based on shape using the following metrics: sphericity and Dice coefficient. Sphericity (Ψ) was used to measure how similar the shape of the VTA was to a sphere [29]. The sphericity of an object ranges from 0 to 1, where 1 corresponds to a sphere by definition. Sphericity was calculated with

$$\Psi = \frac{\pi^{1/3}(6V)^{2/3}}{A}, \tag{2}$$

where V is the volume of the enclosed VTA and A is the surface area of the enclosed VTA. *Enclosed* meant that the lead trajectory through the VTA (Fig. 1c) was filled in for this particular metric.

The Dice coefficient (DC) was used to directly measure the similarity between anisotropic and isotropic VTAs [23]. DC ranges from 0 to 1, where 1 corresponds to identical VTAs. The DC was calculated with

$$DC = \frac{2|V_{iso} \cap V_{aniso}|}{|V_{iso}| + |V_{aniso}|}, \tag{3}$$

where V_{aniso} is the volume of the anisotropic VTA and V_{iso} is the volume of the isotropic VTA.

D. VTA Location Classification

Since the location of therapeutic stimulation was previously found to vary across patients [7], anisotropic VTAs were classified into three groups based on VTA location and VTA-STN overlap relative to the STN centroid in a particular direction (LM, AP, and DV) to assess VTA sensitivity with respect to stimulation location. For example, in the DV direction, a VTA with greater ventral STN overlap than dorsal was labeled a *ventral* VTA (Fig. S1). A VTA that was completely dorsal to the STN (zero overlap) was labeled *dorsal*. If a VTA had approximately equal dorsal and ventral STN overlap (dorsal-ventral ratio equal to 1 after rounding), it was labeled *centered*. A similar approach was used to classify VTAs in the LM and AP directions.

E. Statistical Analysis

Paired, two-sided Wilcoxon signed-rank tests were used to determine if anisotropic VTA volume, LM spread, AP spread, DV spread, and sphericity differed significantly from those of isotropic VTAs. Two-sample t-tests were used (after confirming normality with one-sample Kolmogorov-Smirnov tests) to determine if VTA volume, spread, sphericity, and DC differed significantly based on stimulation location relative to the STN (for example, dorsal/ventral, dorsal/centered, and ventral/centered; similar comparisons were made in the LM and AP directions). Since higher stimulation intensities generate larger VTAs in general [10], [30], VTA volume and spread were divided by the corresponding stimulation amplitude to normalize the metrics. Effect size was calculated using Cohen's d [31] and Rosenthal's formula [32] for the t-tests and Wilcoxon signed-rank tests, respectively. Pearson's linear correlation coefficient was used to assess the relationships between sphericity (proxy for anisotropy, where lower sphericity corresponds to more anisotropic) and VTA volume and spread. Statistical analysis was performed using MATLAB. Significance was determined at a p-value less than 0.05, adjusted for multiple comparisons as needed with the Holm-Bonferroni method.

III. Results

A. Anisotropy Increases VTA Volume and Spread

Anisotropic VTAs (n = 288) exhibited significantly larger volume than isotropic VTAs (n = 288) ($p < 0.001$, Wilcoxon signed-rank test; effect size r = 0.82) (Fig. 2). Individually, this relationship held in 58 implantations (232 electrodes) (Fig. S2). However, 17 anisotropic VTAs (across the other 14 implantations (56 electrodes)) had a smaller volume than their corresponding isotropic VTA. The average volume of anisotropic and isotropic VTAs was 67.66 ± 22.07 mm^3 (mean ± standard deviation) and 55.94 ± 15.34 mm^3, respectively (21.0% increase).

Volume was split into spread in the LM, AP, and DV directions from the VTA centroid. Anisotropic VTAs exhibited significantly larger spread than isotropic VTAs in all three directions ($p < 0.001$, Wilcoxon signed-rank test; effect

This article has been accepted for publication in IEEE Transactions on Biomedical Engineering. This is the author's version which has not been fully edited and content may change prior to final publication. Citation information: DOI 10.1109/TBME.2024.3359119

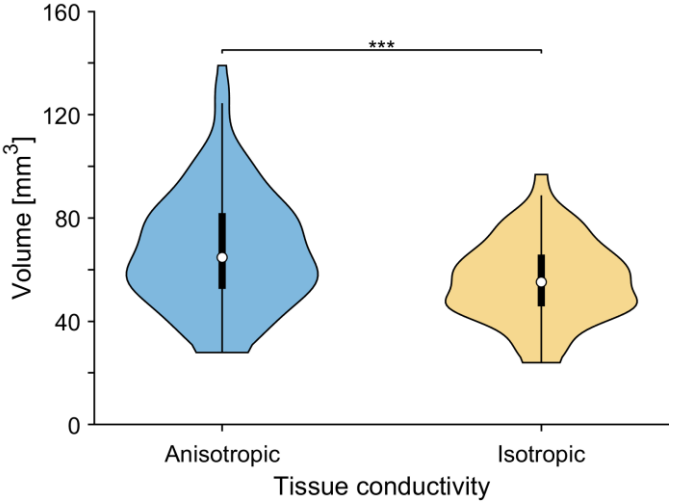

Fig. 2. Volume of anisotropic and isotropic VTAs. Violin plot showing the difference in volume between anisotropic and isotropic VTAs across implantations. *** $p < 0.001$, paired, two-sided Wilcoxon signed-rank test.

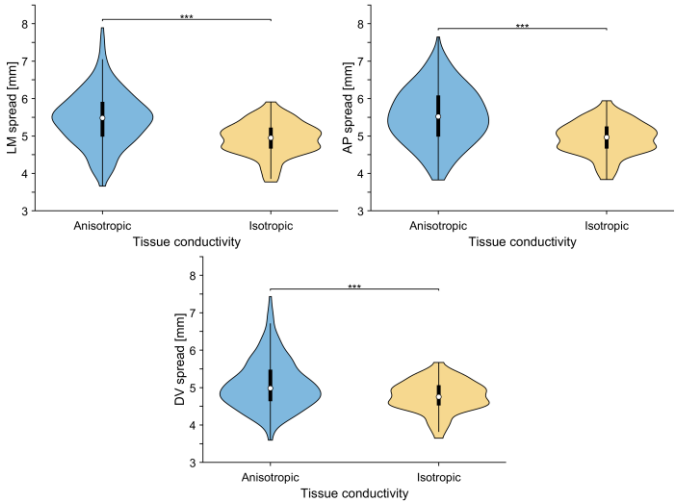

Fig. 3. Spread of anisotropic and isotropic VTAs. Violin plots showing the differences in LM spread (top left), AP spread (top right), and DV spread (bottom) between anisotropic and isotropic VTAs across implantations. *** $p < 0.001$, paired, two-sided Wilcoxon signed-rank test.

size r = 0.78, 0.82, and 0.59 for LM, AP, and DV spread, respectively) (Fig. 3). Individually, this relationship held in 51 implantations (204 electrodes) for LM spread (Fig. S3, top). However, 27 anisotropic VTAs (across the other 21 implantations (84 electrodes)) had a smaller LM spread than their corresponding isotropic VTA. For AP spread, it held in 55 implantations (220 electrodes) (Fig. S3, middle), but 26 anisotropic VTAs (across 17 implantations (68 electrodes)) had a smaller AP spread. For DV spread, it held in 24 implantations (96 electrodes) (Fig. S3, bottom), but 72 anisotropic VTAs (across 48 implantations (192 electrodes)) had a smaller DV spread. The average spread of anisotropic and isotropic VTAs in the LM direction was 5.46 ± 0.72 mm and 4.92 ± 0.45 mm, respectively (10.9% increase); 5.53 ± 0.75 mm and 4.94 ± 0.44 mm, respectively (11.9% increase) in the AP direction; and 5.08 ± 0.66 mm and 4.77 ± 0.41 mm, respectively (6.6% increase) in the DV direction. Interestingly, the extent of variation in anisotropic VTA volume and spread differed across electrodes for each patient and implantation.

B. Lateral and Anterior Stimulation Have Larger LM VTA Spread

Anisotropic VTA volume and spread were normalized by stimulation amplitude to control for differences in stimulation intensity across implantations. For anisotropic VTAs, LM spread differed significantly based on VTA location (relative to the STN centroid) in the LM and AP directions. In the LM direction, VTAs lateral to the STN (n = 99) had significantly larger LM spread than VTAs centered around the STN (n = 54) ($p < 0.01$, t-test) (Fig. 4, top left). The average LM spread of lateral and centered VTAs was 2.23 ± 0.39 mm/V and 2.02 ± 0.27 mm/V, respectively (9.9% difference). In the AP direction, VTAs posterior to the STN (n = 168) had significantly smaller LM spread than VTAs anterior to the STN (n = 87) ($p < 0.001$, t-test) (Fig. 4, top right). The average LM spread of posterior and anterior VTAs was 2.07 ± 0.34 mm/V and 2.23 ± 0.28 mm/V, respectively (7.4% difference).

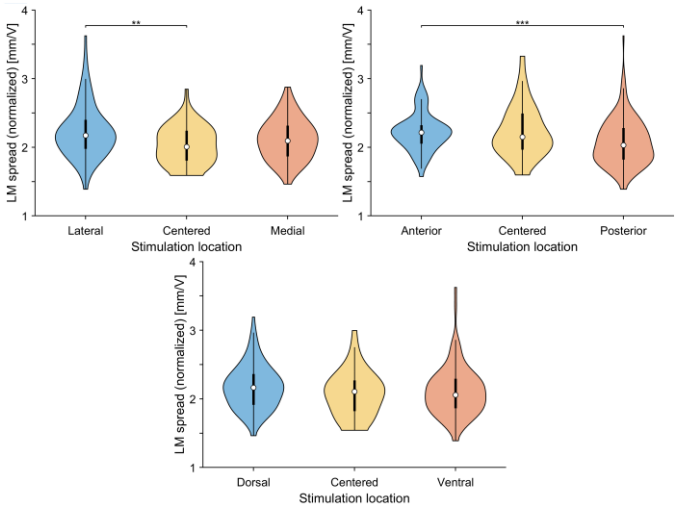

Fig. 4. Normalized LM spread of anisotropic VTAs grouped by their location relative to the STN centroid. Violin plots showing the differences in LM spread in the LM direction (top left), AP direction (top right), and DV direction (bottom) across implantations. ** $p < 0.01$ and *** $p < 0.001$, two-sample t-test.

No significant differences in LM spread in the DV direction (Fig. 4, bottom) and in volume, AP spread, and DV spread in any direction were found.

C. Anisotropy Decreases VTA Sphericity

Across implantations, anisotropic VTAs (n = 288) exhibited significantly lower sphericity than isotropic VTAs (n = 288) ($p < 0.001$, Wilcoxon signed-rank test; effect size r = -0.87) (Fig. 5). Individually, this relationship held in all 72 implantations (288 electrodes) (Fig. S4). The average sphericity of anisotropic and isotropic VTAs was 0.97 ± 0.01 and 0.99 ± 7.94×10^{-4}, respectively (2.0% decrease). Although the sphericity of isotropic VTAs was approximately 1, it was not equal to the theoretical value due to the nonspherical electrode geometry and finite mesh density. Interestingly, the extent of variation in anisotropic VTA sphericity differed across

This article has been accepted for publication in IEEE Transactions on Biomedical Engineering. This is the author's version which has not been fully edited and content may change prior to final publication. Citation information: DOI 10.1109/TBME.2024.3359119

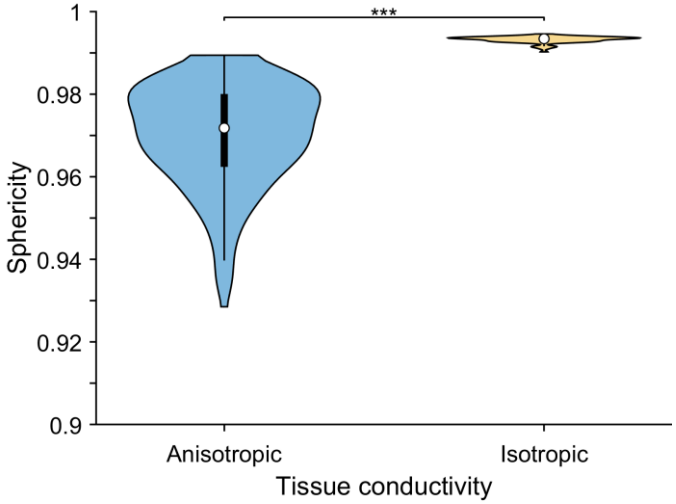

Fig. 5. Sphericity of anisotropic and isotropic VTAs. Violin plot showing the difference in sphericity between anisotropic and isotropic VTAs across implantations. *** $p < 0.001$, paired, two-sided Wilcoxon signed-rank test.

electrodes for each patient and implantation.

D. Dorsal Stimulation Has Higher VTA Sphericity

For anisotropic VTAs, sphericity differed significantly based on VTA location (relative to the STN centroid) in the DV direction. VTAs dorsal to the STN (n = 147) had significantly higher sphericity than VTAs ventral to the STN (n = 97) ($p < 0.001$, t-test; Cohen's d = 0.70) (Fig. 6, left). The average sphericity of dorsal and ventral VTAs was 0.973 ± 0.011 and 0.965 ± 0.012, respectively (0.8% difference). Similarly, the DC between anisotropic and isotropic VTAs differed significantly based on VTA location in the DV direction. VTAs dorsal to the STN had a significantly higher DC than VTAs ventral to the STN ($p < 0.001$, t-test; Cohen's d = 0.47) (Fig. 6, right). The average DC of dorsal and ventral VTAs was 0.82 ± 0.04 and 0.80 ± 0.05, respectively (2.5% difference). Both effect sizes were *medium* according to Cohen [31]. No significant differences in sphericity and DC in the LM and AP directions were found.

E. VTA Sphericity Negatively Correlates With Volume and Spread

A more spherical VTA corresponded to a more isotropic tissue conductivity (Fig. 5). Therefore, the sphericity of anisotropic VTAs was used as a proxy for the degree of tissue anisotropy. Anisotropic VTA volume and spread were correlated with sphericity. Correlation analysis showed a significant negative relationship between sphericity and volume ($r = -0.37$, $p < 0.001$, linear correlation) (Fig. 7), where higher sphericity was associated with smaller VTA volume. Significant negative relationships between sphericity and LM spread, AP spread, and DV spread were also found ($r = -0.35$, -0.50, and -0.47, respectively, $p < 0.001$, linear correlation), where higher sphericity was associated with less VTA spread.

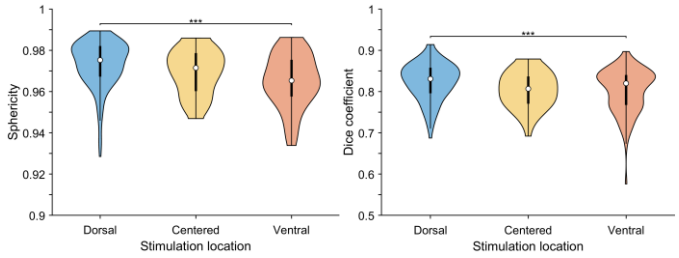

Fig. 6. Sphericity of anisotropic VTAs and the DC between anisotropic and isotropic VTAs grouped by their location relative to the STN centroid. Violin plots showing the differences in sphericity (left) and DC (right) in the DV direction across implantations. *** $p < 0.001$, two-sample t-test.

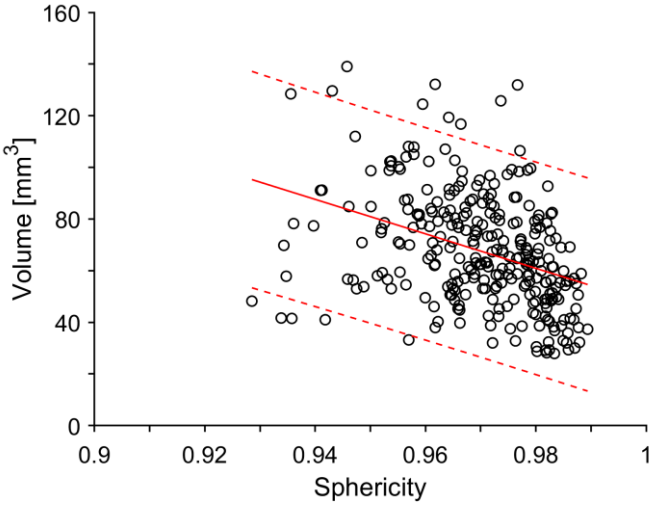

Fig. 7. Negative correlation between sphericity and volume of anisotropic VTAs. The solid and dashed red lines indicate the linear fit and 95% prediction interval, respectively. $r = -0.37$, $p < 0.001$, Pearson's linear correlation coefficient.

IV. Discussion

A. Effect of Anisotropy on VTA Size

Results demonstrated that anisotropic tissue conductivity had a variable effect on VTA size across patients and implantations, with the general trend being that the anisotropic models generated larger VTAs than their isotropic counterparts (Fig. 2). This finding aligns with recent studies evaluating the effect of anisotropy on the VTA [23], [24]. In DBS models for four and one patients, respectively, these studies showed that VTA volume increased with increasing anisotropy. However, another study evaluating the effect of DBS model complexity, which included anisotropy and heterogeneity, on the VTA found the opposite relationship [20]. In a model for one PD patient, this study showed that the most detailed model (anisotropic) performed best, whereas the simpler models (isotropic) overestimated the VTA, by reconciling the VTA predictions with experimental data. Other factors were involved simultaneously, such as the electrode-electrolyte interface and gliosis around the implant, which affect the impedance of the models (in addition to how tissue conductivity was modeled in each domain). Model variations with respect to impedance, in turn, could explain the discrepancy between findings. Controlling for impedance differences using clinical measurements would facilitate

comparisons across studies. In the present study, gliosis was not explicitly modeled (via a layer of lower, homogeneous, and isotropic conductivity) to preserve the patient-specific anisotropic conductivity tensors near the DBS lead and isolate the effect of anisotropy. Notably, the trend of anisotropic models generating larger VTAs did not hold for all implantations as some had anisotropic VTAs with volumes smaller than the isotropic VTA. To further characterize VTA size, the spread of the VTA in the LM, AP, and DV directions was also measured (Fig. 3). Like VTA volume, the general trend was that the anisotropic VTAs spread more than the isotropic VTAs in all three directions. However, the increase in DV spread was less pronounced. The trend of anisotropic VTAs having larger DV spread did not hold as well across implantations compared to LM and AP spreads, suggesting more restricted spread of stimulation in the DV direction. Interestingly, for VTA volume and spread, the dispersion of the anisotropic measurements varied across implantations, suggesting that the subthalamic region in some brain hemispheres may be more isotropic (lower dispersion) than others. Furthermore, [24] showed that the isotropic case did not yield the smallest volume and spread for voltage-controlled stimulation. Variations in the direction of anisotropy across patients and implantations could explain this observed variability. Therefore, incorporating anisotropy in DBS models may matter more depending on the patient and lead location.

Although there were no significant differences in volume, AP spread, and DV spread in any direction after classifying the anisotropic VTAs based on stimulation location, LM spread differed significantly in the LM and AP directions (Fig. 4). More specifically, lateral VTAs had significantly larger LM spread than STN-centered VTAs, which is interesting because the dorsolateral portion of the STN is the conventional DBS target for PD [33]. Just lateral to the STN is the internal capsule (IC), a white matter structure that, when activated, can cause unwanted side effects, such as involuntary muscle contractions and dysarthria [33]. Results suggest that by targeting the lateral half of the STN, there may be an increased likelihood of stimulation spreading laterally to the IC. In the AP direction, posterior VTAs had significantly smaller LM spread than anterior VTAs. The posterior subthalamic area (PSA) is another DBS target for treating tremor syndromes, including tremor-dominant PD [34]. The effectiveness of PSA DBS may partially be explained by this finding, which suggests that the spread of stimulation in the LM direction is more restricted posterior to the STN. Since the PSA contains mainly white matter tracts, and is posterior and medial to the IC [34], the likelihood of stimulation spreading laterally to the IC is decreased. These findings should be considered during DBS programming to prevent side effects resulting from inadvertent IC stimulation.

B. Effect of Anisotropy on VTA Shape

Results also demonstrated that anisotropy had a variable effect on VTA shape across patients and implantations, with the universal trend being that the anisotropic models generated less spherical VTAs than their isotropic counterparts (Fig. 5). Since an isotropic VTA was expected to have a sphericity of approximately 1, this finding makes sense and aligns with previous studies [11], [19], [22]. Qualitatively, anisotropy did not drastically alter the shape of the VTA. This explains the relatively high sphericity (> 0.9) measured for all anisotropic VTAs (for reference, the sphericity of a cube is ≈ 0.8). Despite this, anisotropic VTAs were found to be significantly less spherical than isotropic VTAs. Like for VTA volume and spread, the dispersion of the anisotropic measurements for sphericity varying across implantations stood out.

Although there were no significant differences in the LM and AP directions after classifying the anisotropic VTAs, sphericity differed significantly in the DV direction (Fig. 6). More specifically, dorsal VTAs had significantly higher sphericity than ventral VTAs, which again is interesting because dorsolateral STN is the standard target [33]. This finding suggests that the conductivity of the tissue in the dorsal region of the STN is more isotropic than the tissue conductivity in the ventral STN region, possibly due to multiple crossing fibers. This is supported by the anisotropic-isotropic VTA DC analysis. The implication of this finding is that it may be reasonable to assume uniform stimulation spread in the dorsal STN region. Therefore, for active contacts in or near the dorsal border of the STN, simpler DBS models with homogeneous and isotropic tissue conductivity may be sufficient to accurately predict the VTA and inform stimulation parameter optimization. The same, however, cannot be said for active contacts in the ventral STN region, where the spread of stimulation may be more uneven. This idea may be further supported by investigating the fractional anisotropy in different subthalamic regions.

All VTA size metrics correlated significantly with sphericity, showing negative relationships (Fig. 7). These findings suggest that stimulation may be more confined in isotropic brain regions, and are supported by the VTA size results discussed above and recent studies that investigated the effect of anisotropy on the distribution of the electric field induced by DBS [23], [24]. A limitation mentioned in [23] was the number of samples (4 patients). Although [24] specifically was a theoretical study that used data from one patient as a benchmark, more patients are required to generalize findings. The present study addressed this by including 40 patients, each having their unique anisotropy incorporated in their tissue activation model(s).

C. Clinical Relevance

DBS modeling aims to develop tools that can inform clinical practice and, in turn, improve patient outcomes. For example, preoperative targeting and postoperative programming processes could be refined and optimized using VTA overlap with gray and white matter structures, such as the STN and IC, respectively, alongside clinical evaluations [5]. The VTA is a more accurate measure of stimulation location than active contact position because it considers the

spread of stimulation in all directions [7]. However, as a user-defined metric, its ability to predict DBS outcomes may vary depending on the method used to calculate the VTA.

Commercial DBS software to simulate and visualize the VTA relative to the target structure, such as GUIDE and SureTune, have been approved for clinical use [35]. However, the DBS models employed by these systems typically do not incorporate patient-specific electrical tissue properties, namely anisotropic conductivity, in their calculation of the VTA. The tissue surrounding the lead is instead assumed to be homogeneous and isotropic. A recent study compared VTA predictions from SureTune software to those from homogeneous and heterogeneous DBS models in COMSOL and found that the SureTune VTAs were similar overall to the homogeneous/heterogeneous COMSOL VTAs for voltage-controlled stimulation [35]. Although tissue heterogeneity was considered, anisotropy was not. Another study determined that tissue anisotropy affected the VTA to a greater degree than heterogeneity [18]. The present study investigated this result further by quantifying the influence of anisotropic tissue on VTA predictions in a patient-specific manner. It was found that anisotropy affects VTA size and shape variably across patients and stimulation location. Therefore, clinical decision-making based on VTA predictions from DBS software that do not take the electrical properties of the surrounding tissue into account is likely suboptimal. It is also important to remember that VTA predictions are an estimate of the possible extent of stimulation beyond the active contact for the most excitable neural tissue, based on a theoretical construct. They are not intended to imply that all tissue inside the VTA is activated. VTA predictions ultimately need to be validated experimentally using measurable biomarkers and patient outcomes to establish their clinical utility.

D. Limitations and Future Work

There are limitations that should be considered when interpreting these findings. In common with similar work, image voxel size and coregistration error, number of diffusion gradient directions, electrostatic finite element model solutions, and threshold-based VTA definitions [7] all affect the results. The level of complexity required to sufficiently model the DBS-induced electric field is still uncertain. Tissue anisotropy is one of the more important factors to consider when modeling the VTA [18], but the precise impact of anisotropy on the VTA at the individual level is currently unknown. This is complicated by there being different methods to incorporate anisotropy in DBS models. The Tuch approach [27] is an established method. However, it may overestimate conductivity [18]. Although alternative methods have been proposed, they require further validation. Isolating the effect of tissue anisotropy from tissue heterogeneity is another limitation. In the patient-specific DBS models that incorporated individual DTI data, anisotropy and heterogeneity were difficult to disentangle because each voxel had an essentially unique conductivity tensor associated with it. However, previous studies have reported that heterogeneity has a minor impact on the VTA [18], [35], so its contribution was considered minimal. Normalizing the VTA size metrics by stimulation amplitude for comparison is a limitation as well because they are nonlinearly related. Since VTA size differences due to anisotropy were found proportional to stimulation voltage [3], this approximation was deemed reasonable. However, normalization by amplitude alone may not account for other differences across patients.

Directly affecting VTA predictions is the method used to calculate the VTA. VTA methodologies, such as the axon model, activating function, and electric field norm methods, also vary in complexity [36]. The electric field norm method, based on activation field strength thresholds derived using biophysical axon models [4], was used. By defining VTAs with constant electric field thresholds, computation time was substantially reduced. However, the original thresholds were derived from isotropic conductance models with axons oriented perpendicular to the DBS lead [4]. It is uncertain how thresholds would be affected by DBS models incorporating heterogeneous and anisotropic tissue conductivities [36] or axon models with true fiber orientations [37]. Although the electric field norm and axon model methods have been shown to generate similar VTA predictions for monopolar and voltage-controlled stimulation [4], [36], the effect of patient-specific anisotropy on VTAs calculated using other methodologies remains to be investigated.

Electrode impedance is another factor that affects the VTA. For example, a high-impedance layer of tissue around the active contact will decrease the spread of stimulation and VTA size [30]. Clinical impedance measurements are usually taken to confirm device function and can be used to indirectly assess the state of the electrode-tissue interface [38]. Glial encapsulation of the DBS lead is a primary contributor to impedance. Incorporating encapsulation in DBS models may be helpful for further model validation because it would enable impedance matching between the modeled and clinical measurements (Fig. S5). This would avoid parameter discrepancies in the literature for the conductivity of encapsulation tissue by using a more data-driven approach.

DBS modeling is often used to correlate VTA predictions with measurable clinical outcomes to identify stimulation features associated with the greatest therapeutic benefit (for example, VTA-STN overlap and Unified Parkinson's Disease Rating Scale improvement) [7], [20], [36]. As this study showed, the size and shape of the VTA was significantly influenced by the incorporation of anisotropy in individualized tissue activation models. This finding may, in turn, affect the results of VTA studies investigating the relationship between stimulation location and patient outcome. Although this study did not evaluate and compare the predictive capability of anisotropic and isotropic VTAs with respect to clinical outcomes, doing so is a natural next step. With the use of newer stimulation paradigms, such as current-controlled and directional DBS, anisotropy may play a more prominent role in tissue activation modeling [23], [24].

V. Conclusion

Incorporating patient-specific anisotropic brain conductivity in tissue activation models generated larger and less spherical VTAs. Tissue anisotropy had a variable effect on VTA size and shape across patients and implantations, highlighting the need to consider individualized factors in DBS modeling for accurate VTA characterization. The influence of anisotropy also depended on the local tissue environment in and around the STN, with the dorsal STN region being more isotropic than the ventral STN region (based on VTA analysis), suggesting that the spread of stimulation delivered dorsally more closely resembled the idealized case. In contrast, lateral and posterior stimulation had larger and smaller spreads in the LM direction, respectively. This study quantified the effect of anisotropy on VTA predictions in a patient-specific manner. Its findings, combined with neuroanatomical and clinical information, may aid in identifying optimal stimulation sites on an individual basis.

Acknowledgment

The authors thank the participating patients and A. D. Ahamparam for data visualization assistance.

References

[1] P. S. Larson, "Deep brain stimulation for movement disorders," *Neurotherapeutics*, vol. 11, no. 3, pp. 465–474, May 2014.

[2] N. R. Provenza *et al.*, "The case for adaptive neuromodulation to treat severe intractable mental disorders," *Front. Neurosci.*, vol. 13, p. 152, Feb. 2019.

[3] C. R. Butson *et al*., "Predicting the effects of deep brain stimulation with diffusion tensor based electric field models," *Med. Image Comput. Comput. Assist. Interv.*, vol. 9, no. 2, pp. 429–437, Oct. 2006.

[4] M. Åström *et al*., "Relationship between neural activation and electric field distribution during deep brain stimulation," *IEEE Trans. Biomed. Eng.*, vol. 62, no. 2, pp. 664–672, Feb. 2015.

[5] C. C. McIntyre and T. J. Foutz, "Computational modeling of deep brain stimulation," *Handb. Clin. Neurol.*, vol. 116, pp. 55–61, 2013.

[6] C. R. Butson, "Computational models of neuromodulation," *Int. Rev. Neurobiol.*, vol. 107, pp. 5–22, 2012.

[7] K. A. Malaga *et al.*, "Atlas-independent, N-of-1 tissue activation modeling to map optimal regions of subthalamic deep brain stimulation for Parkinson disease," *Neuroimage. Clin.*, vol. 29, p. 102518, 2021.

[8] K. A. Malaga *et al*., "Thalamic segmentation and neural activation modeling based on individual tissue microstructure in deep brain stimulation for essential tremor," *Neuromodulation*, Dec. 2022.

[9] J. A. Sweet *et al.*, "Computational modeling and neuroimaging techniques for targeting during deep brain stimulation," *Front. Neuroanat.*, vol. 10, no. 71, Jun. 2016.

[10] B. Mädler and V. A. Coenen, "Explaining clinical effects of deep brain stimulation through simplified target-specific modeling of the volume of activated tissue," *AJNR. Am. J. Neuroradiol.*, vol. 33, no. 6, pp. 1072–1080, Jun. 2012.

[11] C. Schmidt and U. van Rienen, "Modeling the field distribution in deep brain stimulation: the influence of anisotropy of brain tissue," *IEEE Trans. Biomed. Eng.*, vol. 59, no. 6, pp. 1583–1592, Jun. 2012.

[12] K. Gunalan *et al.*, "Creating and parameterizing patient-specific deep brain stimulation pathway-activation models using the hyperdirect pathway as an example," *PLoS One*, vol. 12, no. 4, p. e0176132, Apr. 2017.

[13] F. Jiang *et al.*, "Effect of biophysical model complexity on predictions of volume of tissue activated (VTA) during deep brain stimulation," *Annu. Int. Conf. IEEE Eng. Med. Biol. Soc.*, vol. 2020, pp. 3629–3633, Jul. 2020.

[14] C. R. Butson and C. C. McIntyre, "Role of electrode design on the volume of tissue activated during deep brain stimulation," *J. Neural Eng.*, vol. 3, no. 1, pp. 1–8, Mar. 2006.

[15] F. Alonso *et al.*, "Influence on deep brain stimulation from lead design, operating mode and tissue impedance changes – A simulation study," *Brain Disord. Ther.*, vol. 4, no. 3, p. 1000169, Jun. 2015.

[16] R. Erasmi *et al.*, "White matter changes along the electrode lead in patients treated with deep brain stimulation," *Front. Neurol.*, vol. 9, no. 983, Nov. 2018.

[17] D. P. Floden *et al.*, "Contact location and neuropsychological outcomes in subthalamic deep brain stimulation," *Neurosurgery*, vol. 83, no. 4, pp. 666–674, Oct. 2018.

[18] B. Howell and C. C. McIntyre, "Analyzing the tradeoff between electrical complexity and accuracy in patient-specific computational models of deep brain stimulation," *J. Neural Eng.*, vol. 13, no. 3, p. 036023, Jun. 2016.

[19] C. Ineichen *et al.*, "Understanding the effects and adverse reactions of deep brain stimulation: Is it time for a paradigm shift toward a focus on heterogenous biophysical tissue properties instead of electrode design only?," *Front. Hum. Neurosci.*, vol. 12, no. 468, Nov. 2018.

[20] A. Chaturvedi *et al.*, "Patient-specific models of deep brain stimulation: influence of field model complexity on neural activation predictions," *Brain Stimul.*, vol. 3, no. 2, pp. 65–77, Apr. 2010.

[21] J. Volkmann *et al.*, "Basic algorithms for the programming of deep brain stimulation in Parkinson's disease," *Mov. Disord.*, vol. 21, no. Suppl 14, pp. S284–S289, Jun. 2006.

[22] M. Åström *et al.*, "Influence of heterogeneous and anisotropic tissue conductivity on electric field distribution in deep brain stimulation," *Med. Biol. Eng. Comput.*, vol. 50, no. 1, pp. 23–32, Jan. 2012.

[23] T. Nordin *et al.*, "White matter tracing combined with electric field simulation – A patient-specific approach for deep brain stimulation," *Neuroimage. Clin.*, vol. 24, p. 102026, 2019.

[24] T. Nordin *et al*., "The effect of anisotropy on the impedance and electric field distribution in deep brain stimulation," *IFMBE Proc.*, vol. 80, pp. 1069–1077, 2021.

[25] P. G. Patil *et al.*, "The anatomical and electrophysiological subthalamic nucleus visualized by 3-T magnetic resonance imaging," *Neurosurgery*, vol. 71, no. 6, pp. 1089–1095, Dec. 2012.

[26] L. Houshmand, "Optimized targeting in deep brain stimulation for movement disorders," Ph.D. dissertation, Dept. Biomed. Eng., Univ. of MI, Ann Arbor, MI, 2015.

[27] D. S. Tuch *et al.*, "Conductivity tensor mapping of the human brain using diffusion tensor MRI," *Proc. Natl. Acad. Sci. U. S. A.*, vol. 98, no. 20, pp. 11697–11701, Sep. 2001.

[28] A. R. Kent and W. M. Grill, "Analysis of deep brain stimulation electrode characteristics for neural recording," *J. Neural Eng.*, vol. 11, no. 4, p. 046010, Jun. 2014.

[29] H. Wadell, "Volume, shape, and roundness of quartz particles," *J. Geol.*, vol. 43, no. 3, pp. 250–280, May 1935.

[30] C. R. Butson *et al.*, "Sources and effects of electrode impedance during deep brain stimulation," *Clin. Neurophysiol.*, vol. 117, no. 2, pp. 447–454, Feb. 2006.

[31] J. Cohen, *Statistical Power Analysis for the Behavioral Sciences*, 2nd ed. New York: Lawrence Erlbaum Associates, 1988.

[32] R. Rosenthal, "Parametric measures of effect size," in *The handbook of research synthesis.* Russell Sage Foundation, 1994, pp. 231–244.

[33] P. van den Munckhof *et al.*, "Targeting of the subthalamic nucleus in patients with Parkinson's disease undergoing deep brain stimulation surgery," *Neurol. Ther.*, vol. 10, no. 1, pp. 61–73, Jun. 2021.

[34] A. Ramirez-Zamora *et al*., "Evolving concepts in posterior subthalamic area deep brain stimulation for treatment of tremor: surgical neuroanatomy and practical considerations," *Stereotact. Funct. Neurosurg.*, vol. 94, no. 5, pp. 283–297, Oct. 2016.

[35] J. D. Johansson and P. Zsigmond, "Comparison between patient-specific deep brain stimulation simulations and commercial system SureTune3," *Biomed. Phys. Eng. Express*, vol. 7, no. 5, Jul. 2021.

[36] G. Duffley *et al.*, "Evaluation of methodologies for computing the deep brain stimulation volume of tissue activated," *J. Neural Eng.*, vol. 16, no. 6, p. 066024, Oct. 2019.

[37] J. P. Slopsema *et al*., "Clinical deep brain stimulation strategies for orientation-selective pathway activation," *J. Neural Eng.*, vol. 15, no. 5, p. 056029, Sep. 2018.

[38] C. Lungu *et al.*, "Temporal macrodynamics and microdynamics of the postoperative impedance at the tissue-electrode interface in deep brain stimulation patients," *J. Neurol. Neurosurg. Psychiatry*, vol. 85, no. 7, pp. 816–819, Jul. 2014.